EUROPEAN LABORATORY FOR PARTICLE PHYSICS

CERN-PPE/96-103
23 July 1996

A study of τ decays involving η and ω mesons

The ALEPH Collaboration

Abstract

The 132 pb^{-1} of data collected by ALEPH from 1991 to 1994 have been used to analyze η and ω production in τ decays. The following branching fractions have been measured:

$$\begin{aligned} B(\tau^- \to \nu_\tau \omega h^-) &= (1.91 \pm 0.07 \pm 0.06) \times 10^{-2}, \\ B(\tau^- \to \nu_\tau \omega h^- \pi^0) &= (4.3 \pm 0.6 \pm 0.5) \times 10^{-3}, \\ B(\tau^- \to \nu_\tau \eta K^-) &= (2.9^{+1.3}_{-1.2} \pm 0.7) \times 10^{-4}, \\ B(\tau^- \to \nu_\tau \eta h^- \pi^0) &= (1.8 \pm 0.4 \pm 0.2) \times 10^{-3} \end{aligned}$$

and the 95% C.L. limit $B(\tau^- \to \nu_\tau \eta \pi^-) < 6.2 \times 10^{-4}$ has been obtained. The $\omega\pi^-$ and $\eta\pi^-\pi^0$ rates and dynamics are found in agreement with the predictions made from e^+e^- annihilation data with the help of isospin invariance (CVC).

To be submitted to Zeitschrift für Physik

The ALEPH Collaboration

D. Buskulic, I. De Bonis, D. Decamp, P. Ghez, C. Goy, J.-P. Lees, A. Lucotte, M.-N. Minard, J.-Y. Nief, P. Odier, B. Pietrzyk

Laboratoire de Physique des Particules (LAPP), IN^{2}P^3-CNRS, 74019 Annecy-le-Vieux Cedex, France

M.P. Casado, M. Chmeissani, J.M. Crespo, M. Delfino, I. Efthymiopoulos,[1] E. Fernandez, M. Fernandez-Bosman, Ll. Garrido,[15] A. Juste, M. Martinez, S. Orteu, C. Padilla, I.C. Park, A. Pascual, J.A. Perlas, I. Riu, F. Sanchez, F. Teubert

Institut de Fisica d'Altes Energies, Universitat Autonoma de Barcelona, 08193 Bellaterra (Barcelona), Spain[7]

A. Colaleo, D. Creanza, M. de Palma, G. Gelao, M. Girone, G. Iaselli, G. Maggi, M. Maggi, N. Marinelli, S. Nuzzo, A. Ranieri, G. Raso, F. Ruggieri, G. Selvaggi, L. Silvestris, P. Tempesta, A. Tricomi,[3] G. Zito

Dipartimento di Fisica, INFN Sezione di Bari, 70126 Bari, Italy

X. Huang, J. Lin, Q. Ouyang, T. Wang, Y. Xie, R. Xu, S. Xue, J. Zhang, L. Zhang, W. Zhao

Institute of High-Energy Physics, Academia Sinica, Beijing, The People's Republic of China[8]

R. Alemany, A.O. Bazarko, G. Bonvicini,[23] P. Bright-Thomas, M. Cattaneo, P. Comas, P. Coyle, H. Drevermann, R.W. Forty, M. Frank, R. Hagelberg, J. Harvey, P. Janot, B. Jost, E. Kneringer, J. Knobloch, I. Lehraus, G. Lutters, E.B. Martin, P. Mato, A. Minten, R. Miquel, Ll.M. Mir,[2] L. Moneta, T. Oest,[20] A. Pacheco, J.-F. Pusztaszeri, F. Ranjard, P. Rensing,[12] G. Rizzo, L. Rolandi, D. Schlatter, M. Schmelling,[24] M. Schmitt, O. Schneider, W. Tejessy, I.R. Tomalin, A. Venturi, H. Wachsmuth, A. Wagner

European Laboratory for Particle Physics (CERN), 1211 Geneva 23, Switzerland

Z. Ajaltouni, A. Barrès, C. Boyer, A. Falvard, P. Gay, C . Guicheney, P. Henrard, J. Jousset, B. Michel, S. Monteil, J-C. Montret, D. Pallin, P. Perret, F. Podlyski, J. Proriol, P. Rosnet, J.-M. Rossignol

Laboratoire de Physique Corpusculaire, Université Blaise Pascal, IN^{2}P^3-CNRS, Clermont-Ferrand, 63177 Aubière, France

T. Fearnley, J.B. Hansen, J.D. Hansen, J.R. Hansen, P.H. Hansen, B.S. Nilsson, B. Rensch, A. Wäänänen

Niels Bohr Institute, 2100 Copenhagen, Denmark[9]

A. Kyriakis, C. Markou, E. Simopoulou, I. Siotis, A. Vayaki, K. Zachariadou

Nuclear Research Center Demokritos (NRCD), Athens, Greece

A. Blondel, G. Bonneaud, J.C. Brient, P. Bourdon, A. Rougé, M. Rumpf, A. Valassi,[6] M. Verderi, H. Videau[21]

Laboratoire de Physique Nucléaire et des Hautes Energies, Ecole Polytechnique, IN^{2}P^3-CNRS, 91128 Palaiseau Cedex, France

D.J. Candlin, M.I. Parsons

Department of Physics, University of Edinburgh, Edinburgh EH9 3JZ, United Kingdom[10]

E. Focardi,[21] G. Parrini

Dipartimento di Fisica, Università di Firenze, INFN Sezione di Firenze, 50125 Firenze, Italy

M. Corden, C. Georgiopoulos, D.E. Jaffe

Supercomputer Computations Research Institute, Florida State University, Tallahassee, FL 32306-4052, USA [13,14]

A. Antonelli, G. Bencivenni, G. Bologna,[4] F. Bossi, P. Campana, G. Capon, D. Casper, V. Chiarella, G. Felici, P. Laurelli, G. Mannocchi,[5] F. Murtas, G.P. Murtas, L. Passalacqua, M. Pepe-Altarelli

Laboratori Nazionali dell'INFN (LNF-INFN), 00044 Frascati, Italy

L. Curtis, S.J. Dorris, A.W. Halley, I.G. Knowles, J.G. Lynch, V. O'Shea, C. Raine, P. Reeves, J.M. Scarr, K. Smith, P. Teixeira-Dias, A.S. Thompson, F. Thomson, S. Thorn, R.M. Turnbull

Department of Physics and Astronomy, University of Glasgow, Glasgow G12 8QQ,United Kingdom[10]

U. Becker, C. Geweniger, G. Graefe, P. Hanke, G. Hansper, V. Hepp, E.E. Kluge, A. Putzer, M. Schmidt, J. Sommer, H. Stenzel, K. Tittel, S. Werner, M. Wunsch

Institut für Hochenergiephysik, Universität Heidelberg, 69120 Heidelberg, Fed. Rep. of Germany[16]

D. Abbaneo, R. Beuselinck, D.M. Binnie, W. Cameron, P.J. Dornan, A. Moutoussi, J. Nash, J.K. Sedgbeer, A.M. Stacey, M.D. Williams

Department of Physics, Imperial College, London SW7 2BZ, United Kingdom[10]

G. Dissertori, P. Girtler, D. Kuhn, G. Rudolph

Institut für Experimentalphysik, Universität Innsbruck, 6020 Innsbruck, Austria[18]

A.P. Betteridge, C.K. Bowdery, P. Colrain, G. Crawford, A.J. Finch, F. Foster, G. Hughes, T. Sloan, M.I. Williams

Department of Physics, University of Lancaster, Lancaster LA1 4YB, United Kingdom[10]

A. Galla, I. Giehl, A.M. Greene, C. Hoffmann, K. Jakobs, K. Kleinknecht, G. Quast, B. Renk, E. Rohne, H.-G. Sander, P. van Gemmeren, C. Zeitnitz

Institut für Physik, Universität Mainz, 55099 Mainz, Fed. Rep. of Germany[16]

J.J. Aubert,[21] A.M. Bencheikh, C. Benchouk, A. Bonissent, G. Bujosa, D. Calvet, J. Carr, C. Diaconu, F. Etienne, N. Konstantinidis, P. Payre, D. Rousseau, M. Talby, A. Sadouki, M. Thulasidas, K. Trabelsi

Centre de Physique des Particules, Faculté des Sciences de Luminy, IN^{2}P^3-CNRS, 13288 Marseille, France

M. Aleppo, F. Ragusa[21]

Dipartimento di Fisica, Università di Milano e INFN Sezione di Milano, 20133 Milano, Italy

C. Bauer, R. Berlich, W. Blum, V. Büscher, H. Dietl, F. Dydak,[21] G. Ganis, C. Gotzhein, H. Kroha, G. Lütjens, G. Lutz, W. Männer, H.-G. Moser, R. Richter, A. Rosado-Schlosser, S. Schael, R. Settles, H. Seywerd, R. St. Denis, H. Stenzel, W. Wiedenmann, G. Wolf

Max-Planck-Institut für Physik, Werner-Heisenberg-Institut, 80805 München, Fed. Rep. of Germany[16]

J. Boucrot, O. Callot, Y. Choi,[26] A. Cordier, M. Davier, L. Duflot, J.-F. Grivaz, Ph. Heusse, A. Höcker, A. Jacholkowska, M. Jacquet, D.W. Kim,[19] F. Le Diberder, J. Lefrançois, A.-M. Lutz, I. Nikolic, H.J. Park,[19] M.-H. Schune, S. Simion, J.-J. Veillet, I. Videau, D. Zerwas

Laboratoire de l'Accélérateur Linéaire, Université de Paris-Sud, IN^{2}P^3-CNRS, 91405 Orsay Cedex, France

P. Azzurri, G. Bagliesi, G. Batignani, S. Bettarini, C. Bozzi, G. Calderini, M. Carpinelli, M.A. Ciocci, V. Ciulli, R. Dell'Orso, R. Fantechi, I. Ferrante, L. Foà,[1] F. Forti, A. Giassi, M.A. Giorgi, A. Gregorio, F. Ligabue, A. Lusiani, P.S. Marrocchesi, A. Messineo, F. Palla, G. Sanguinetti, A. Sciabà, P. Spagnolo, J. Steinberger, R. Tenchini, G. Tonelli,[25] C. Vannini, P.G. Verdini, J. Walsh

Dipartimento di Fisica dell'Università, INFN Sezione di Pisa, e Scuola Normale Superiore, 56010 Pisa, Italy

G.A. Blair, L.M. Bryant, F. Cerutti, J.T. Chambers, Y. Gao, M.G. Green, T. Medcalf, P. Perrodo, J.A. Strong, J.H. von Wimmersperg-Toeller

Department of Physics, Royal Holloway & Bedford New College, University of London, Surrey TW20 OEX, United Kingdom[10]

D.R. Botterill, R.W. Clifft, T.R. Edgecock, S. Haywood, P. Maley, P.R. Norton, J.C. Thompson, A.E. Wright

Particle Physics Dept., Rutherford Appleton Laboratory, Chilton, Didcot, Oxon OX11 OQX, United Kingdom[10]

B. Bloch-Devaux, P. Colas, S. Emery, W. Kozanecki, E. Lançon, M.C. Lemaire, E. Locci, B. Marx,

P. Perez, J. Rander, J.-F. Renardy, A. Roussarie, J.-P. Schuller, J. Schwindling, A. Trabelsi, B. Vallage

CEA, DAPNIA/Service de Physique des Particules, CE-Saclay, 91191 Gif-sur-Yvette Cedex, France[17]

S.N. Black, J.H. Dann, R.P. Johnson, H.Y. Kim, A.M. Litke, M.A. McNeil, G. Taylor

Institute for Particle Physics, University of California at Santa Cruz, Santa Cruz, CA 95064, USA[22]

C.N. Booth, R. Boswell, C.A.J. Brew, S. Cartwright, F. Combley, A. Koksal, M. Letho, W.M. Newton, J. Reeve, L.F. Thompson

Department of Physics, University of Sheffield, Sheffield S3 7RH, United Kingdom[10]

A. Böhrer, S. Brandt, G. Cowan, C. Grupen, J. Minguet-Rodriguez, F. Rivera, P. Saraiva, L. Smolik, F. Stephan,

Fachbereich Physik, Universität Siegen, 57068 Siegen, Fed. Rep. of Germany[16]

M. Apollonio, L. Bosisio, R. Della Marina, G. Giannini, B. Gobbo, G. Musolino

Dipartimento di Fisica, Università di Trieste e INFN Sezione di Trieste, 34127 Trieste, Italy

J. Rothberg, S. Wasserbaech

Experimental Elementary Particle Physics, University of Washington, WA 98195 Seattle, U.S.A.

S.R. Armstrong, P. Elmer, Z. Feng,[27] D.P.S. Ferguson, Y.S. Gao,[28] S. González, J. Grahl, T.C. Greening, O.J. Hayes, H. Hu, P.A. McNamara III, J.M. Nachtman, W. Orejudos, Y.B. Pan, Y. Saadi, I.J. Scott, A.M. Walsh,[29] Sau Lan Wu, X. Wu, J.M. Yamartino, M. Zheng, G. Zobernig

Department of Physics, University of Wisconsin, Madison, WI 53706, USA[11]

---

[1] Now at CERN, 1211 Geneva 23, Switzerland.
[2] Supported by Dirección General de Investigación Científica y Técnica, Spain.
[3] Also at Dipartimento di Fisica, INFN, Sezione di Catania, Catania, Italy.
[4] Also Istituto di Fisica Generale, Università di Torino, Torino, Italy.
[5] Also Istituto di Cosmo-Geofisica del C.N.R., Torino, Italy.
[6] Supported by the Commission of the European Communities, contract ERBCHBICT941234.
[7] Supported by CICYT, Spain.
[8] Supported by the National Science Foundation of China.
[9] Supported by the Danish Natural Science Research Council.
[10] Supported by the UK Particle Physics and Astronomy Research Council.
[11] Supported by the US Department of Energy, grant DE-FG0295-ER40896.
[12] Now at Dragon Systems, Newton, MA 02160, U.S.A.
[13] Supported by the US Department of Energy, contract DE-FG05-92ER40742.
[14] Supported by the US Department of Energy, contract DE-FC05-85ER250000.
[15] Permanent address: Universitat de Barcelona, 08208 Barcelona, Spain.
[16] Supported by the Bundesministerium für Forschung und Technologie, Fed. Rep. of Germany.
[17] Supported by the Direction des Sciences de la Matière, C.E.A.
[18] Supported by Fonds zur Förderung der wissenschaftlichen Forschung, Austria.
[19] Permanent address: Kangnung National University, Kangnung, Korea.
[20] Now at DESY, Hamburg, Germany.
[21] Also at CERN, 1211 Geneva 23, Switzerland.
[22] Supported by the US Department of Energy, grant DE-FG03-92ER40689.
[23] Now at Wayne State University, Detroit, MI 48202, USA.
[24] Now at Max-Plank-Institüt für Kernphysik, Heidelberg, Germany.
[25] Also at Istituto di Matematica e Fisica, Università di Sassari, Sassari, Italy.
[26] Permanent address: Sung Kyun Kwon University, Suwon, Korea.
[27] Now at The Johns Hopkins University, Baltimore, MD 21218, U.S.A.
[28] Now at Harvard University, Cambridge, MA 02138, U.S.A.
[29] Now at Rutgers University, Piscataway, NJ 08855-0849, U.S.A.

1 Introduction

Using 132 pb^{-1} of data collected by the ALEPH detector from 1991 to 1994, the τ decay modes with an η or ω meson and one or two π mesons have been studied. This allows, for the relevant channels, a refinement of the global determination of the τ hadronic branching fractions already performed by ALEPH [1].

Decay modes involving η have been the subject of many theoretical studies [2, 3, 4, 5] and it has been pointed out [3] that the $\eta\pi$ and $\omega\pi$ decay modes are good places to look for "second-class" currents [6] for which the correlation between G parity and J^P quantum numbers is reversed. From the experimental side, the knowledge of the production of resonances with electromagnetic decays, like η and ω, is necessary for a complete understanding of the τ decay modes.

In the present study, the ω is reconstructed from its three-pion decay and the η from both the two-photon and three-pion decays. In order to improve the efficiencies and to check their evaluation, events in which the two photons from a π^0 are merged in the calorimeter are also retained as well as events in which one of the two photons is lost. Therefore the following seven topologies[1] are studied:

$$
\begin{array}{lcccl}
\eta\pi^- & \rightarrow & & & \pi^-\gamma\gamma \\
 & \searrow & & & \\
\omega\pi^- & \rightarrow & \pi^+\pi^-\pi^-\pi^0 & \rightarrow & \left\{ \begin{array}{l} \pi^+\pi^-\pi^-\gamma\gamma \\ \pi^+\pi^-\pi^-\gamma(\gamma) \end{array} \right. \\
 & & & & \\
\eta\pi^-\pi^0 & \rightarrow & \pi^-\pi^0\gamma\gamma & \rightarrow & \left\{ \begin{array}{l} \pi^-\gamma\gamma\gamma\gamma \\ \pi^-\gamma\gamma\gamma(\gamma) \end{array} \right. \\
 & \searrow & & & \\
\omega\pi^-\pi^0 & \rightarrow & \pi^+\pi^-\pi^-\pi^0\pi^0 & \rightarrow & \left\{ \begin{array}{l} \pi^-\pi^-\pi^+\gamma\gamma\gamma\gamma \\ \pi^-\pi^-\pi^+\gamma\gamma\gamma(\gamma) \end{array} \right. \quad ,
\end{array}
$$

which correspond to one charged track and two to four photons and three charged tracks and one to four photons.

The number of observed $Z \rightarrow q\bar{q}$ decays and the Z branching ratios are used for normalization.

2 The ALEPH detector

A detailed description of the ALEPH detector and its performance can be found in Ref. [7, 8]. The present analysis uses mainly the tracking subcomponents and the electromagnetic calorimeter (ECAL). It takes full advantage of the high granularity of the ECAL.

Charged tracks are measured by a silicon vertex detector (VDET) with two-dimensional readout, a cylindrical multiwire drift chamber (ITC) and a large time projection chamber (TPC) which also measures the ionization (dE/dx). The three detectors are immersed in a 1.5 T axial magnetic field and together provide a transverse momentum resolution $\sigma(1/p_T) = 0.6 \times 10^{-3}\,(\mathrm{GeV/c})^{-1}$.

[1] The charge conjugate configuration is always implied. Except for the $\eta\pi/K$ channels, no distinction is made between $\pi^\pm$ and $K^\pm$; in the following sections the letter h will stand for π or K.

The ECAL is a lead/proportional chamber sandwich of 45 layers, segmented into $13 \times 13\,\mathrm{mrad}^2$ projective towers which are read out in three sections of depth of 4, 9 and 9 radiation lengths respectively. An energy resolution of $\sigma(E)/E = (18/\sqrt{E(\mathrm{GeV})} \oplus 2)\,\%$ is achieved.

The hadron calorimeter (HCAL), a 23-layer iron/streamer tubes sandwich, and two additional double layer muon chambers allow the identification of muons.

3 Particle identification

3.1 Charged particle identification

Specialized algorithms, optimized for τ physics, have been designed to discriminate hadrons, electrons and muons [1, 9]. The method used here is described in Ref. [9] where it is referred to as LM method. Electron-hadron separation uses information from the dE/dx measurement in the TPC and shower energy and shape in the ECAL. The muon chambers and HCAL responses are used to distinguish hadrons from muons. The efficiencies for particle identification have been checked on samples of hadrons, electrons and muons from data and Monte Carlo.

In the ηh^- channel the π K separation uses the dE/dx measurement as described in Ref. [1, 10].

3.2 Photon and π^0 reconstruction

Photons are detected as showers in the ALEPH electromagnetic calorimeter or by their materialization as electron pairs [7, 8].

The algorithms used to construct the clusters of ECAL cells associated to a shower

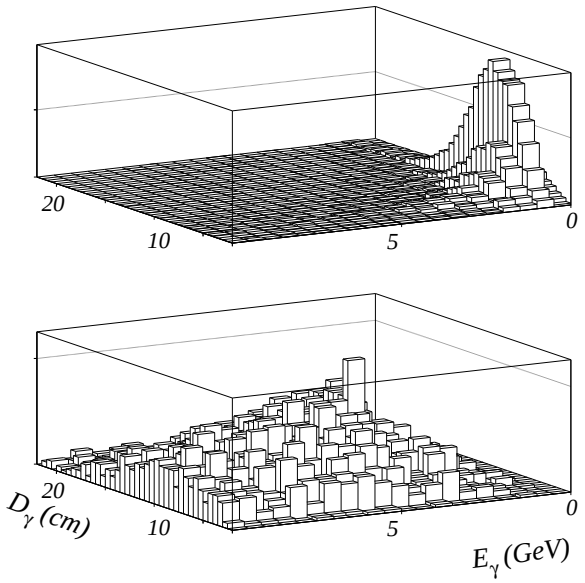

Figure 1: Distribution in the plane (E_γ,D_γ) (arbitrary units) from Monte Carlo samples, for fake photons in $\tau^- \to \nu_\tau \pi^- \pi^- \pi^+$ decays (above), and for real photons in $\tau^- \to \nu_\tau \pi^- \pi^- \pi^+ \pi^0$ decays (below).

and to identify the converted pairs are described in Ref. [8].

Before selection, clusters constructed by the ECAL algorithm include debris of hadronic interactions in the ECAL and subclusters due to fluctuations of the showers. To perform the selection of genuine photons and reject fake photons [1, 9], the characteristics of the clusters are used. The most discriminant variables are the energy (E_γ), the distance to the nearest impact of a charged track (D_γ) and the fraction of the energy deposited in each segment in depth. The separation of genuine and fake photons using these characteristics is illustrated by Fig. 1.

The correct assignment of the ECAL cells to neighbouring clusters and the elimination of satellites is also important in the case of close photons, particularly for the $h\eta\pi^0$ final state where the background from $h\pi^0\pi^0$ is large. More detailed information on clusters is used to reject the satellites. This includes the energy deposited on the border region between two clusters and the distance of the maximum energy cell with respect to the nearest cluster. The efficiencies of the selection procedures have been measured on data and Monte Carlo event samples and the agreement of data and Monte Carlo in the selected region has been checked.

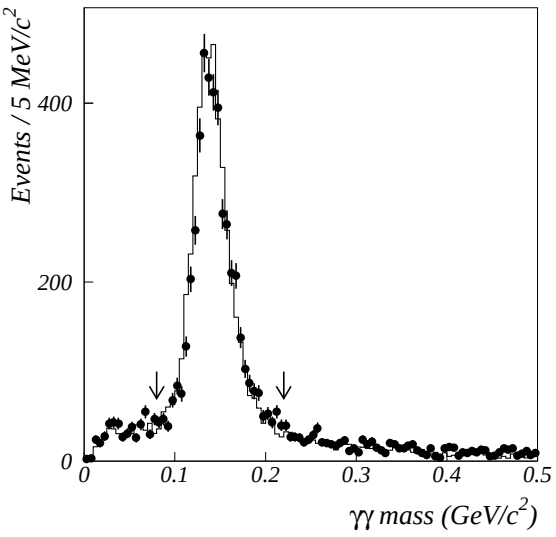

Figure 2: $\gamma\gamma$ mass in $3h^\pm\gamma\gamma$ final state. The black dots are the data and the histogram the Monte Carlo expectation. The cut used to select π^0's is indicated by arrows.

Figure 2 displays the $\gamma\gamma$ invariant mass for three-prong decays. It shows the width of the π^0 peak due to the ECAL resolution. The π^0 energy measurement is improved by means of a kinematic fit of the $\gamma\gamma$ pairs [8] taking into account the angular bias on high energy π^0's due to the finite size of ECAL cells and the clustering algorithm. The χ^2 of the fit is used in multiphoton events to select (or reject when looking for η) the $\gamma\gamma$ combinations.

The systematic errors on the branching ratios due to γ and π^0 reconstruction are estimated by varying the selection criteria and adding in quadrature the variations of the result.

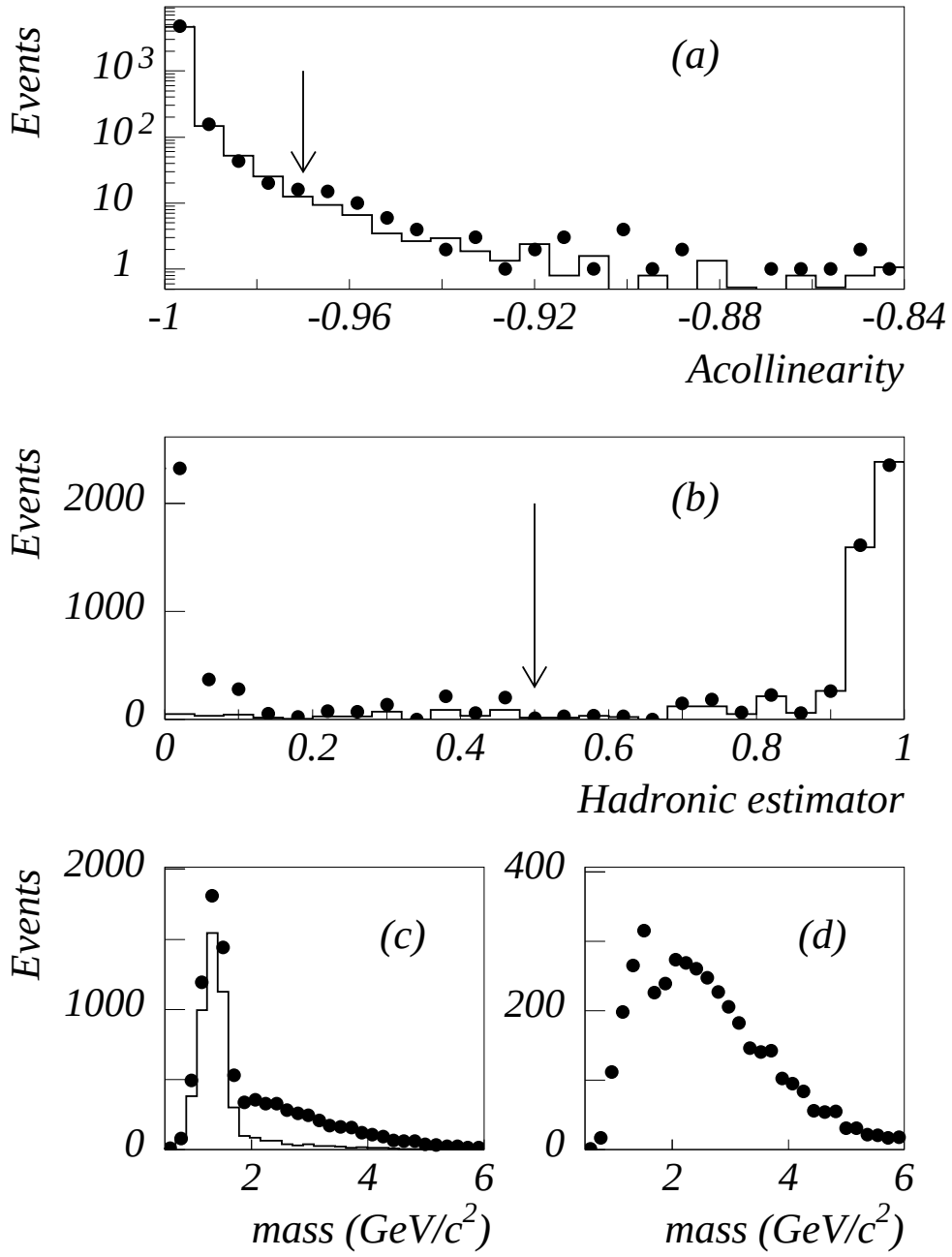

Figure 3: Distributions used in the selection of three-prong decays; the arrows indicate the position of the cuts: (a) acollinearity, (b) hadronic ($q\bar{q}$) estimator measured in the recoil hemisphere. For (a) and (b) the points represent data and the histogram the $\tau\tau$ Monte Carlo. (c) total mass in the selected hemisphere before (points) and after (histogram) the cut on the hadronic estimator. (d) the same for events rejected by the cut.

4 Event selection

The first step is a loose preselection which keeps almost all the $Z \to l^+l^-$ decays in the angular acceptance of the detector. This preselection, described in Ref. [9], retains events with charged track multiplicity between two and eight and requires $|\cos\theta| < 0.9$ for the thrust angle θ computed with charged tracks.

The events are then decomposed into two halves, called hemispheres, according to the thrust axis and the hemispheres are classified using charged track multiplicity, particle identification and γ multiplicity. A cut on the acollinearity between the two hemispheres (Fig. 3a) is performed to reject the $\gamma\gamma$ background. As already mentioned in the introduction, the hemispheres retained to look for η or ω must contain one charged hadron and two to four γ's or three charged hadrons and one to four γ's since, in order to get a better global acceptance and check the evaluation of the photon detection efficiency, π^0's with only one detected decay γ are also used.

To further reduce the non-tau background without introducing a bias on the studied hemisphere, the opposite hemisphere (recoil hemisphere) is used. Likelihood estimators using only the recoil hemisphere information like charged track and γ multiplicities, energy, mass and particle identification are constructed by the method already used for particle identification [9, 15] in order to distinguish $\tau\tau$ from hadronic ($q\bar{q}$) events and from Bhabha events. They are normalized to be close to one for $\tau\tau$ events and close to 0 for the background. An example of the use of these estimators is given in Fig. 3. A cut on the estimator rejects the background. Reversing the cut one can select background samples and study their characteristics. From the number of events with a total hadronic mass in the selected hemisphere greater than m_τ, it is then possible to estimate directly the $q\bar{q}$ background without relying on a $q\bar{q}$ Monte Carlo. Finally cuts on the total mass of the selected hemisphere are performed.

To evaluate the efficiencies and τ backgrounds, the KORALZ [11] $\tau\tau$ Monte Carlo with updated τ branching ratios [1] has been used. The number of generated Monte Carlo events is four times the number of real events.

5 The $\omega\, h^-$ final state

5.1 The $\tau^- \to \nu_\tau \omega\, h^-$ branching ratio

Both three-prong one-photon and three-prong two-photon events are used and the two samples are independently analysed.

	$1-\gamma$ sample	$2-\gamma$ sample
Number of events	2510	3293
Efficiency (%)	18.07	24.50
τ background (%)	12.85	9.66
Non-τ background (%)	0.70	0.50
$B(\tau^- \to \nu_\tau 3h^\pm\pi^0)$ (%)	$4.22 \pm 0.10 \pm 0.11$	$4.24 \pm 0.08 \pm 0.08$
f_ω (%)	$38.1 \pm 2.4 \pm 1.9$	$41.1 \pm 1.7 \pm 1.2$
$B(\tau^- \to \nu_\tau \omega h^-)$ (%)	$1.81 \pm 0.11 \pm 0.10$	$1.96 \pm 0.08 \pm 0.07$

Table 1: Characteristics of the one- and two-photon samples in the $3h^\pm\pi^0$ channel.

For two-photon candidates, the selection is made by a cut on the $\gamma\gamma$ mass (80 MeV/c^2 < $m_{\gamma\gamma}$ <220 MeV/c^2) and a kinematic fit of the π^0 is performed; for one-photon decays the γ energy is required to be greater than 2.5 GeV. The main results of the two analyses are given in Table 1.

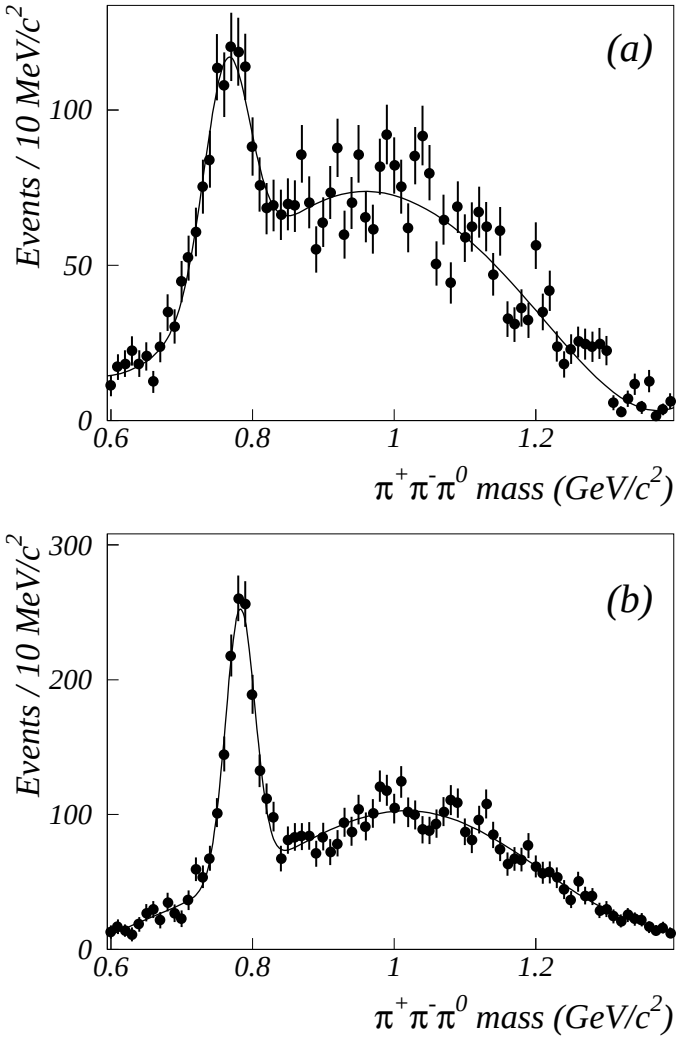

Figure 4: $\pi^+\pi^-\pi^0$ mass distributions (two entries per event) in the $\pi^\pm\pi^+\pi^-\pi^0$ final state for the one-photon sample (a) and the two-photon sample (b). The bin size has been chosen to display the detailed shape of the ω peak. The non-resonant contribution is represented by a simple polynomial. Non-τ background has been subtracted.

The KORALZ [11] $\tau\tau$ Monte Carlo has been used to evaluate the efficiencies and τ backgrounds. Several matrix elements have been tried, as explained below, to study the sensitivity to the dynamics of the decay. The non-τ background is measured using the recoil hemisphere and the total hadronic mass as explained in section 4.

The ω fractions (f_ω) are obtained from fits of the $\pi^+\pi^-\pi^0$ mass distributions shown in Fig. 4. Different parametrizations of the non-resonant contribution (polynomials

and Monte Carlo shapes) have been used. All give ω mass and resolution in good agreement with the Monte Carlo expectations. The variation of the fit result with the parametrization is taken as a systematic error on f_ω.

The agreement between all the results of the two analyses is excellent as well as the agreement with the value $B(\tau^- \to \nu_\tau 3h^\pm\pi^0) = (4.30 \pm 0.09 \pm 0.09)\,\%$, obtained by a largely independent analysis [1] of a part of the same data.

The details of the systematic errors on the branching ratios and the ω fraction are presented in Tables 2 and 3. The main contributions come from the uncertainties

$\Delta B/B$ (%)

	$1-\gamma$ sample	$2-\gamma$ sample
Normalization	0.20	0.20
Non-τ background	0.15	0.16
τ background	0.71	0.76
Dynamics and M.C. stat	1.80	1.06
Tracking	$<$0.54	$<$0.54
Interactions	$<$ 0.50	$<$ 0.50
γ reconstruction	1.7	1.0
π^0 reconstruction	-	0.7
Total	2.65	1.88

Table 2: Systematic errors on the branching ratio of the $\tau^- \to \nu_\tau 3h^\pm\pi^0$ decay channel.

$\Delta f_\omega/f_\omega$ (%)

	$1-\gamma$ sample	$2-\gamma$ sample
Non-τ background	0.3	0.2
ω fraction in τ back.	0.2	0.2
Dynamics and M.C. stat.	3.9	2.7
Fit and parametrization	3.0	1.2
Total	5.0	2.9

Table 3: Systematic errors on the ω fraction measurement in the $\tau^- \to \nu_\tau 3h^\pm\pi^0$ decay channel.

on the models used to simulate the decay dynamics and the mass spectrum fit. The contribution from the γ and π^0 reconstruction described in section 3, though relevant, is less important. The modelling of the dynamics of the non-ω events will be discussed in section 5.3. Its contribution to the systematic errors has been investigated by generating Monte Carlo events with modified matrix elements. Uncertainties on the matrix element and Monte Carlo statistical errors contribute to both $B(\tau \to \nu 4\pi)$ and f_ω and to some extent, cancel in $B(\tau \to \nu\omega h)$ since the dynamics of the $\tau \to \nu\omega h$ decay is well known. For this reason they are put together in the same row in Tables 2 and 3.

The $\omega\pi^-$ branching ratio obtained by the combination of the two analyses is

$$B(\tau^- \to \nu_\tau \omega h^-) = (1.91 \pm 0.07 \pm 0.06)\,\%, \qquad (1)$$

where the correlations of the systematic errors between the two samples as well as between $B(\tau \to \nu 4\pi)$ and f_ω have been taken into account. This value is in good agreement with the measurement by the CLEO collaboration [12]: $(1.95 \pm 0.07 \pm 0.11)\,\%$. Both values are consistent with the estimates obtained from e^+e^- annihilation data by isospin considerations (CVC): $(1.79 \pm 0.14)\,\%$ [13]. The measurements in τ decay are now more accurate than the estimations from e^+e^- annihilation.

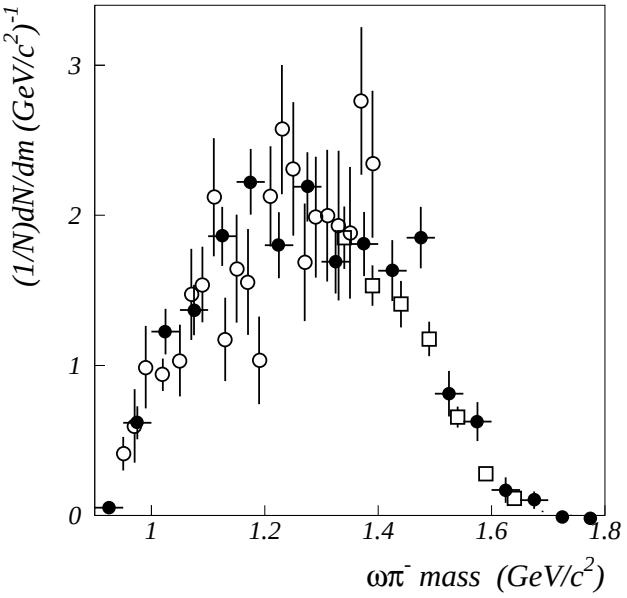

Figure 5: Background-subtracted $\omega\pi$ mass spectrum. Black dots are the data presented here, open circles are the data from the ND experiment and open squares from the DM2 experiment [14].

Isospin invariance predicts not only the branching ratio but also the $\omega\pi$ mass (m) distribution by the relation [13]

$$\frac{1}{N}\frac{dN}{dm} = \frac{B(\tau \to e\nu\bar{\nu})}{B(\tau \to \nu\omega\pi)}\frac{3|V_{ud}|^2}{\pi\alpha^2 m_\tau^8} F(m)\sigma_{e^+e^-\to\omega\pi}(m), \qquad (2)$$

with $F(m) = m^3(m_\tau^2 - m^2)^2(m_\tau^2 + 2m^2)$. A comparison of the present data with e^+e^- annihilation data [14] normalized with respect to the τ leptonic branching ratio [15] is shown on Fig. 5 after background subtraction estimated from side bands and good agreement is found. The mass dependence of the efficiency is found to be almost constant.

5.2 Spin parity of the ωh^- system

In the standard model, the $\omega\pi^-$ system is produced by the vector current and must have spin-parity $J^P = 1^-$ quantum numbers. Checking this prediction is a way to put limits on the above-mentioned non-standard second-class currents.

Defining the ω decay angle χ as the angle, in the ω rest frame, between the normal to the ω decay plane and the direction of the fourth pion, the decay distribution is predicted to be $(3/4)\sin^2\chi$ for a $J^P = 1^-$, ωh^- system.

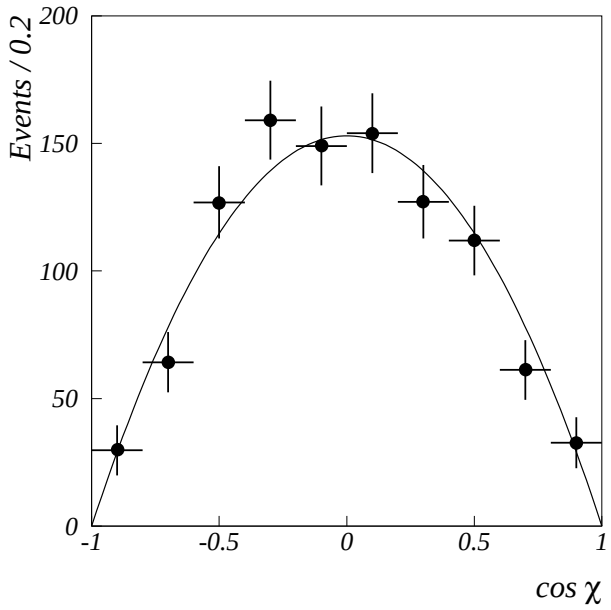

Figure 6: Background-subtracted ω decay distribution (see text). The curve is the $\sin^2\chi$ predicted for a $J^P = 1^-$ $\omega\pi^-$ system.

To construct the decay distribution, the non-ω background is first reduced by a cut on the three-pion Dalitz plot. Its contribution, estimated from the sidebands in the three-pion mass distribution, is then subtracted from the $\cos\chi$ distribution in the ω peak. The experimental distribution of $\cos\chi$, shown in Fig. 6, is clearly consistent with the standard model prediction. For $J^P = 0^-$ or $J^P = 1^+$ systems the expected distribution is $3(1 + c\cos^2\chi)/2(c + 3)$ with $c \geq 0$. Assuming $c = 0$ which is the most conservative hypothesis, a fit of the experimental distribution with $1/4[3(1-\epsilon)\sin^2\chi + 2\epsilon]$ gives a limit on the contribution ϵ of second-class currents.

Taking into account the systematic errors due to the uncertainties on the background and acceptances the limit given by the fit is

$$\epsilon < 0.086 \quad (95\,\%\ \text{C.L.}). \tag{3}$$

5.3 The non-$\omega\pi$ contribution

The model used in TAUOLA [11], the standard tau decay Monte Carlo, is the implementation of a chiral dynamics inspired model [16] for $\rho\pi\pi$ production which predicts no ρ^- in a τ^- decay and a ratio $\rho^+/\rho^0 = 2$.

The dominant ρ production is clear from the $\pi\pi$ mass spectra (Fig. 7) for non-ω events. A simultaneous fit to the four ($\pi^0\pi^+$, $\pi^+\pi^-$, $\pi^0\pi^-$ and $\pi^-\pi^-$) $\pi\pi$ mass spectra has been performed [17] assuming an incoherent mixture of the three charge states

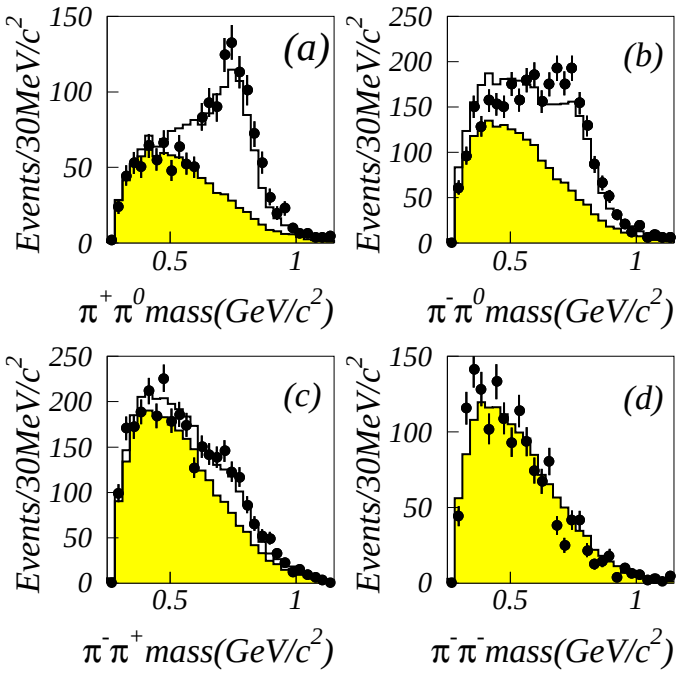

Figure 7: $\pi\pi$ mass distributions for events without ω, (a) and (d) one entry per event, (b) and (c) two entries per event. Data are shown as black dots and the result of the fit as a histogram. For each charge combination, the shaded histogram is the contribution of ρ's of different charge.

of the ρ, but taking into account kinematical reflections and Bose symmetrization. It shows that the non-ω events are consistent with 100 % $\rho\pi\pi$ production but not with the predicted charge ratios. With the constraint $W_{\rho^-} + W_{\rho^+} + W_{\rho^0} = 1$, the fractions of ρ^+ and ρ^- in τ^- decay are found to be $W_{\rho^+} = 0.42 \pm 0.02\,(stat.)$ and $W_{\rho^-} = 0.38 \pm 0.02\,(stat.)$ but the oversimplified model and the poor quality of the fit indicate that systematic errors on the ρ production measurements are large.

A recent theoretical analysis [18] improving on [16] predicts ρ fractions in qualitative agreement with the present findings. Nevertheless a complete understanding of the final state would require a dedicated study.

Variations of the W values compatible with the fit have been used to estimate the systematic errors on the $\omega\pi$ branching ratio due to the poor knowledge of the dynamics for non-ω events.

6 The $\omega\, h^-\pi^0$ final state

As already mentioned, both three-prong three-photon and three-prong four-photon events are used to look for the $\omega h^\pm\pi^0$ decay mode. The association of photons into π^0 candidates is based on the χ^2 of the π^0 fit. The relevant numbers for those final states are summarized in Table 4. The branching ratios are in excellent agreement with the measurement $B(\tau^- \to \nu_\tau 3h^\pm 2\pi^0) = (5.0 \pm 0.7 \pm 0.7) \times 10^{-3}$, obtained by a largely independent analysis [1] of a part of the same data.

	$3-\gamma$ sample	$4-\gamma$ sample
Number of events	459	269
Efficiency (%)	15.7	13.3
τ background (%)	43.7	26.0
Non-τ background (%)	1.5	2
$B(\tau^- \to \nu_\tau 3h^\pm 2\pi^0)(10^{-3})$	$5.7 \pm 0.5 \pm 0.7$	$5.1 \pm 0.4 \pm 0.4$

Table 4: Characteristics of the three- and four-photon samples in the $3h^\pm 2\pi^0$ channel.

Due to the limited statistics, the 3γ and 4γ samples are used together to construct the $\pi^+\pi^-\pi^0$ mass spectrum of Fig. 8. The non-τ background has been measured from the data as explained in section 4 and subtracted from the spectrum.

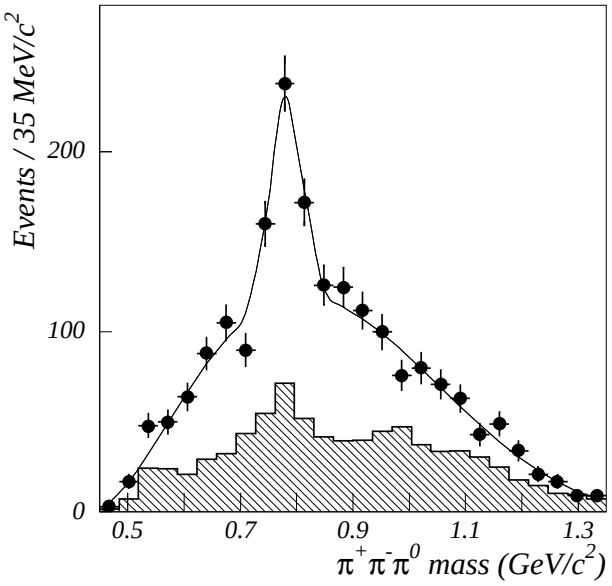

Figure 8: $\pi^+\pi^-\pi^0$ mass distributions in the $3h^-\pi^0\pi^0$ final state (four entries per event). The non-τ background has been subtracted; the hatched histogram is the background from other τ decay modes.

The ω production is clearly visible in Fig. 8. A fit to the spectrum is performed, where the shape of the non-resonant component is taken to be phase space multiplied by a low order polynomial and the width of the signal is fixed to the value expected from Monte Carlo. It yields the value $(71.5 \pm 8.4 \pm 7.6)\,\%$ for the ω fraction. This value of the ω fraction is combined with the 5π branching ratios, taking into account the correlations of systematic errors. The result is

$$B(\tau^- \to \nu_\tau \omega h^- \pi^0) = (4.3 \pm 0.6 \pm 0.5) \times 10^{-3}. \qquad (4)$$

The value is in good agreement with the CLEO measurement $B(\tau^- \to \nu_\tau \omega h^- \pi^0) = (3.9 \pm 0.4 \pm 0.4) \times 10^{-3}$ [19].

The details of the systematic errors are given in Table 5. An important source of uncertainty is related to the contamination by other tau decay channels and the uncertainty of their ω content. The not well known decay channel $3\pi^\pm 3\pi^0$ gives a large contribution to the sytematic error of the 4γ sample. Since the ω fraction in this final state is unknown, the isospin inequality $\omega\,\pi^- 2\pi^0 \leq \omega\, 3\pi^\pm$ [20] and the well measured $\tau \to \nu_\tau\, 5\pi^\pm \pi^0$ branching ratio are used to limit the ω contribution in the background.

$\Delta B/B$ (%)

	$3h^\pm 2\pi^0$ [4γ]	$3h^\pm 2\pi^0$ [3γ]	$\omega h^- \pi^0$
γ reconstruction	2	10	4
π^0 reconstruction	4	4	7
τ background	6	4	7
Others	1	1	1
Parametrization of the fit	–	–	6
Total	7.5	11.7	12.4

Table 5: Systematic errors for the $3h^\pm 2\pi^0$ channel. Others represents the small contributions detailed in Table 2.

7 The $\eta\,\pi^-$ and $\eta\,K^-$ final states

The clearest signature of an ηh ($h = \pi/K$) decay mode is a peak in the $\gamma\gamma$ mass spectrum for the configuration of one charged track and two photons. For an $\eta\pi$ system of spin J the parity is $P = (-1)^J$ and the G-parity $G = -1$, so it must be produced by a second-class current and such a τ decay is excluded in the standard model to the extent that isospin is conserved. Since there is no such restriction for the strange final state $K\eta$, it is important to distinguish the π from the K. For this purpose, the TPC dE/dx measurement is used to define a K probability P_K in the way described in [10].

The selected events have the one-prong two-photon topology. Such events are dominated by $\tau^- \to \rho^-, K^{*-}\,\nu_\tau$ decays [1] but, for high $\gamma\gamma$ masses, $\tau^- \to h^- 2\pi^0\,\nu_\tau$ decays with two lost photons are the dominant contribution to the background. To reduce it the cut $E_{\gamma 1} + E_{\gamma 2} > 5\,\mathrm{GeV}$ is added to the γ selection cuts. The overall efficiency of the selection, including the P_K cuts, is 50.9 % for a hypothetical $\tau \to a_0^- \nu_\tau / a_0^- \to \eta\pi^-$ decay and 47.7 % for $\tau \to K^-\eta\nu$ assuming a resonant $K^*(1410) \to K\eta$ system.

Figure 9 displays the $\gamma\gamma$ mass spectra for events with high and low K probability. There is some evidence of η production for high P_K and none for low P_K. The fit of a linear combination of Monte Carlo distributions for signal and background to the observed distributions gives a branching fraction

$$B(\tau^- \to \nu_\tau \eta K^-) = (2.9^{+1.3}_{-1.2} \pm 0.7) \times 10^{-4}. \qquad (5)$$

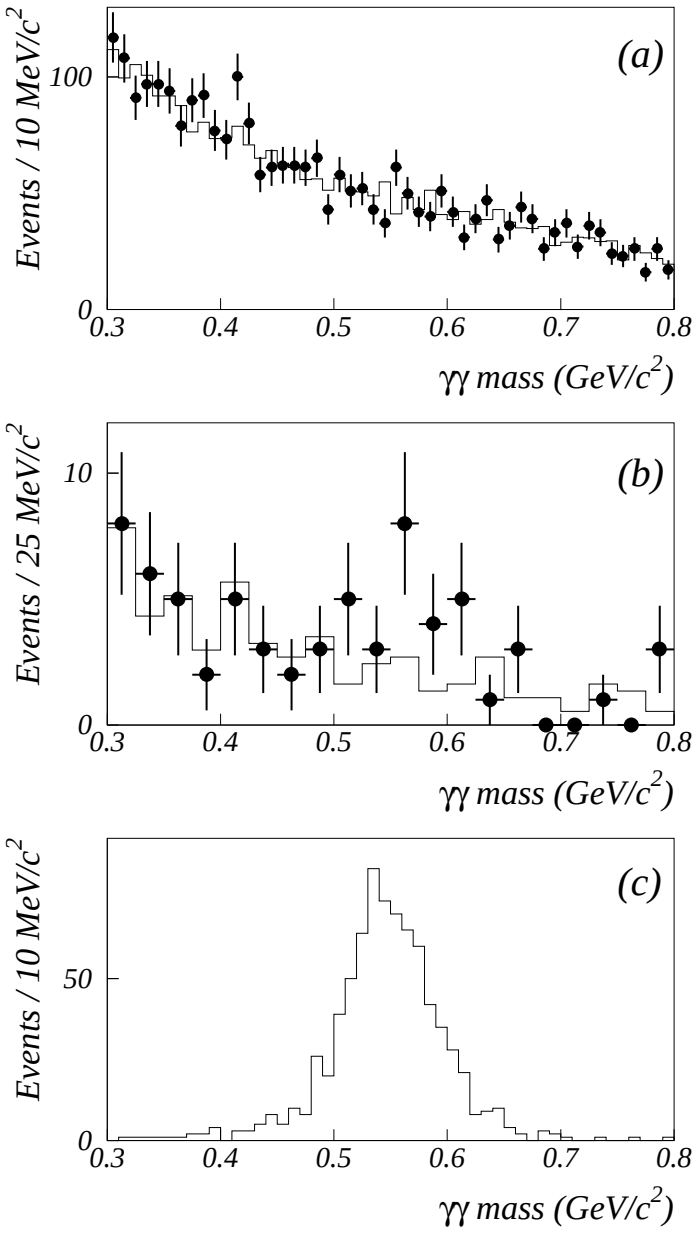

Figure 9: $\gamma\gamma$ mass distributions in the $h\gamma\gamma$ final state: (a) low K probability events, (b) high K probability events (the histograms are the expectations from a Monte Carlo without η); (c) signal expected from $\eta\pi$ Monte Carlo.

for the ηK channel, where the dominant contributions to the systematic error come from the γ reconstruction ($\Delta B/B = 18\,\%$), the P_K normalisation ($\Delta B/B = 10\,\%$) and the uncertainty on the background shape ($\Delta B/B = 10\,\%$).

For the $\eta\pi$ final state, a similar procedure gives a 95% C.L. Bayesian upper limit

$$B(\tau^- \to \nu_\tau \eta \pi^-) < 6.2 \times 10^{-4} \quad (95\%\ \text{C.L.}) \tag{6}$$

taking into account the systematic errors. An ηh decay mode would also contribute to the three-prong one-π^0 channel studied in section 5 but the limit obtained there is only at the level of 2×10^{-3}.

The ηK branching ratio is compatible with the value obtained by the CLEO Collaboration [21]: $B(\tau^- \to \nu_\tau \eta K^-) = (2.6 \pm 0.5 \pm 0.4) \times 10^{-4}$. The ηK branching ratio is of the same order of magnitude as theoretical estimates [4] while limits on $\eta\pi$ are still one order of magnitude above the values deduced from the isospin violation due to the $m_d - m_u$ quark mass difference [2, 4].

8 The $\eta\, h^-\pi^0$ final state

As explained in the introduction, the $\eta\pi\pi$ final state can be searched for in four of the seven studied configurations.

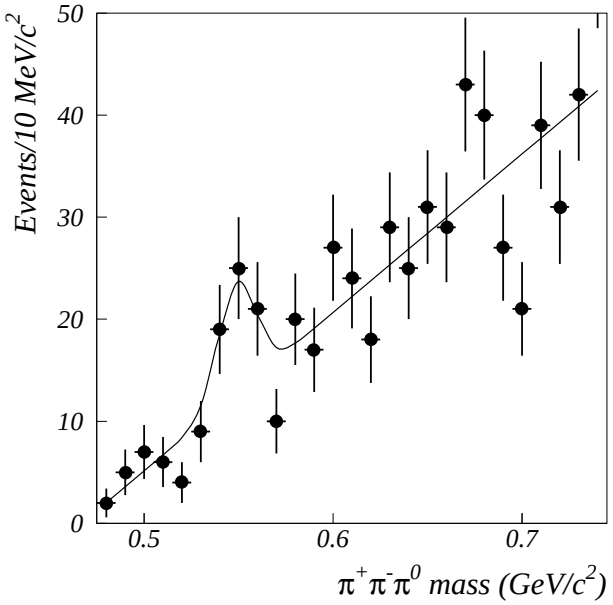

Figure 10: $\pi^+\pi^-\pi^0$ mass distribution in the $3h^-\pi^0\pi^0$ final state (detail of the low mass region of Fig. 8) with the fit of the η signal.

For the three-prong configurations, the relevant spectrum is that shown in Fig. 8 whose low mass region is enlarged in Fig. 10. The efficiency for the three-prong configurations is 33 %. A fit of this histogram to a linear background plus a Gaussian signal whose width is taken from the Monte Carlo yields the measurement $B(\tau^- \to \nu_\tau \eta h^- \pi^0) = (2.4 \pm 0.8 \pm 0.2) \times 10^{-3}$.

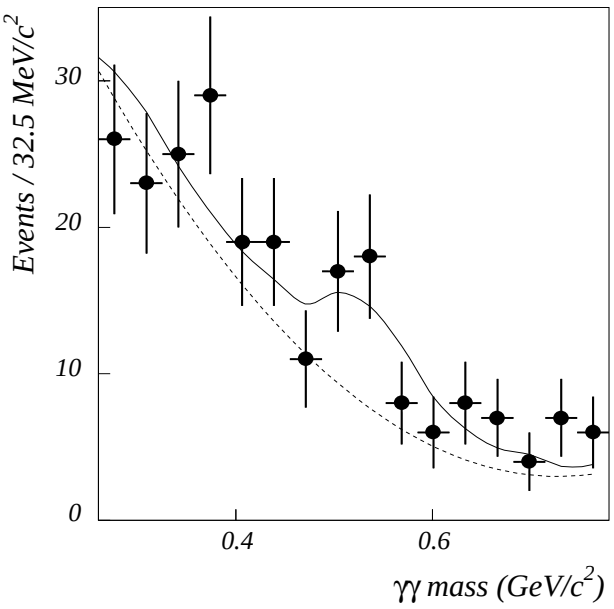

Figure 11: $\gamma\gamma$ mass distribution in the $h\gamma\gamma\gamma$ sample after rejection of candidates consistent with the π^0 hypothesis. The solid curve is the result of the fit; the dashed curve the background given by the fit.

The other configurations are the one-prong three-photon and the one-prong four-photon. The dominant background here is the combinatorial background from $\tau^- \to h^-\pi^0\pi^0$ events. To reduce it, events compatible with the $\pi^0\pi^0$ hypothesis in the 4γ channel and with the $\gamma\pi^0$ hypothesis in the 3γ channel are rejected on the basis of the π^0 fit χ^2. The overall selection efficiencies are 26.8 % for the three-photon sample and 17.4 % for the four-photon sample.

The η production in the three-photon sample is measured by means of a fit to the $\gamma\gamma$ mass spectrum (three entries per decay), shown in Fig. 11, of a linear combination of the Monte Carlo expectations for signal and background. For the 4γ sample, the same procedure is applied to the two-dimensional spectrum (three entries per decay) of the quantities $(m^h_{\gamma\gamma} - m_\eta)/\sigma_\eta$ and $(m^l_{\gamma\gamma} - m_{\pi^0})/\sigma_{\pi^0}$ where $m^l_{\gamma\gamma}$ and $m^h_{\gamma\gamma}$ are the lower and higher $\gamma\gamma$ masses for each of the three combinations. The fits yield the measurements: $B(\tau^- \to \nu_\tau \eta h^- \pi^0) = (1.7 \pm 0.7 \pm 0.2) \times 10^{-3}$ (3-γ) and $B(\tau^- \to \nu_\tau \eta h^- \pi^0) = (1.3 \pm 0.8 \pm 0.4) \times 10^{-3}$ (4-γ).

The dominant systematic errors come from:

- the cut against $\pi^0\pi^0$: $\Delta B/B = 7$ % for the three-photon sample and 15 % for the four-photon sample;
- the uncertainties on the background shape: $\Delta B/B = 15$ %;
- the Monte Carlo statistics for the signal simulation $\Delta B/B = 14$ %.

The combination of the three measurements, taking into account the correlation of

systematic errors, gives the value

$$B(\tau^- \to \nu_\tau \eta h^- \pi^0) = (1.8 \pm 0.4 \pm 0.2) \times 10^{-3}. \quad (7)$$

This value is in good agreement with the measurement by the CLEO collaboration [22]: $(1.7 \pm 0.2 \pm 0.2) \times 10^{-3}$ and slightly higher but consistent with the estimation obtained from e^+e^- annihilation data by isospin considerations (CVC): $(1.3 \pm 0.18) \times 10^{-3}$ [13].

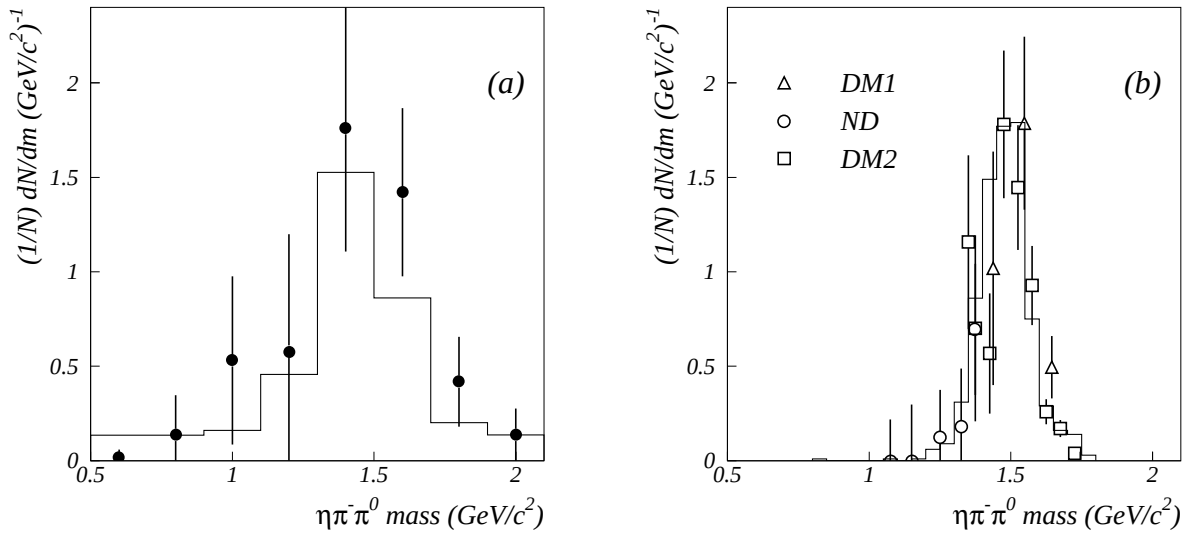

Figure 12: The $\eta\pi\pi^0$ mass spectrum. (a) The points are the data after background subtraction, the histogram the expected distribution from Monte Carlo. (b) The points are computed from e^+e^- annihilation data [23], the histogram is the distribution generated in Monte Carlo before experimental effects.

The hadronic mass distribution is also predicted from e^+e^- data [23] by Eq. 2. Due to the poor resolution on the $\eta\pi\pi$ mass a direct comparison of data is not possible. Figure 12 (a) presents the comparison of τ decay data, after background subtraction, with the Monte Carlo distribution taking into account acceptance and resolution and Fig. 12 (b) the comparison of e^+e^- data with the Monte Carlo generated distribution before experimental effects. Except for the already mentioned slight difference in normalization, the prediction from CVC is in agreement with the present data.

9 Conclusion

The following τ branching fractions have been measured:

$$\begin{aligned} B(\tau^- \to \nu_\tau \omega\ h^-) &= (1.91 \pm 0.07 \pm 0.06) \times 10^{-2} \\ B(\tau^- \to \nu_\tau \omega h^- \pi^0) &= (4.3 \pm 0.6 \pm 0.5) \times 10^{-3} \\ B(\tau^- \to \nu_\tau \eta K^-) &= (2.9^{+1.3}_{-1.2} \pm 0.7) \times 10^{-4} \\ B(\tau^- \to \nu_\tau \eta h^- \pi^0) &= (1.8 \pm 0.4 \pm 0.2) \times 10^{-3} \end{aligned}$$

and the limit

$$B(\tau^- \to \nu_\tau \eta \pi^-) < 6.2 \times 10^{-4} \quad (95\%\ \text{C.L.})$$

has been obtained. They are consistent with previous measurements by the CLEO Collaboration [12, 19, 21, 22].

For the $\omega\pi$ and $\eta\pi\pi$ channels, both the branching ratios and the shapes of the hadronic mass distribution are in agreement with estimates obtained from e^+e^- annihilation data by isospin considerations (CVC) [13].

The J^P quantum numbers of the $\omega\pi$ system are 1^-, as predicted by the standard model. A 95 % C.L. limit on the second-class currents contribution, $\epsilon \leq 0.086$, is obtained.

Acknowledgments

We wish to thank our colleagues in the CERN accelerator divisions for the successful operation of LEP. We are indebted to the engineers and technicians in all our institutions for their contribution to the excellent performance of ALEPH. Those of us from non-member countries thank CERN for its hospitality.

References

[1] ALEPH Collaboration, D. Buskulic et al., Z. Phys. C 70 (1996) 579; ALEPH Collaboration, D. Decamp et al., Z. Phys. C 54 (1992) 211.

[2] S. Tisserant and T.N. Truong, Phys. Lett. 115B (1982) 264; A. Bramon, S. Narison and A. Pich, Phys. Lett. B 196 (1987) 543; C. K. Zachos and Y. Meurice, Mod. Phys. Lett. A 2 (1987) 247; H. Neufeld and H. Rupertsberger, Z. Phys. C 68 (1995) 91.

[3] C. Leroy and J. Pestieau, Phys. Lett. 72B (1978) 398; N. Paver and D. Treleani, Nuovo Cimento Lett. 31 (1981) 364; E.L. Berger and H.J. Lipkin, Phys. Lett. B 189 (1987) 233.

[4] A. Pich, Phys. Lett. B 196 (1987) 561; G.J. Aubrecht II, N. Chahrouri and K. Slanec, Phys. Rev. D 24 (1981) 1318.

[5] G. Kramer and W. F. Palmer, Z. Phys. C 25 (1984) 195; C 39 (1988) 423; E. Braaten, R. J. Oakes, and S. M. Tse, Phys. Rev. D 36 (1987) 2188.

[6] S. Weinberg, Phys. Rev. 112 (1958) 1375.

[7] ALEPH Collaboration, D. Decamp et al., Nucl. Instr. and Methods A286 (1991) 121.

[8] ALEPH Collaboration, D. Buskulic et al., Nucl. Instr. and Methods A360 (1995) 481.

[9] ALEPH Collaboration, D. Buskulic et al., Z. Phys. C 69 (1996) 183; C 59 (1993) 369.

[10] ALEPH Collaboration, D. Buskulic et al., Phys. Lett. B 332 (1994) 209.

[11] S. Jadach, B.F.L. Ward and Z. Wąs, Comp. Phys. Comm. 79 (1994) 503;
S. Jadach et al., Comp. Phys. Comm. 76 (1993) 361.

[12] CLEO Collaboration, R. Balest et al., Phys. Rev. Lett. 75 (1995) 3809.

[13] S.I. Eidelman and V.N. Ivanchenko, Proc. TAU94, ed. L. Rolandi, Nucl. Phys. B 40 (Proc. Suppl.) (1995) 131.

[14] DM2 collaboration, D.Bisello et al., Nucl. Phys. B 21 (Proc. Supp.) (1991) 111;
ND collaboration, S.I. Dolinski et al., Phys. Rep. 202 (1991) 99.

[15] ALEPH Collaboration, D. Buskulic et al., Z. Phys. C 70 (1996) 561.

[16] R. Fischer, J. Wess and F. Wagner, Z. Phys. C 3 (1980) 313.

[17] P. Bourdon, Proc. TAU94, ed. L. Rolandi, Nucl. Phys. B 40 (Proc. Suppl.) (1995) 203.

[18] R. Decker et al., Z. Phys. C 70 (1996) 247.

[19] CLEO Collaboration, D. Bortoletto et al., Phys. Rev. Lett. 71 (1993) 1791.

[20] A. Rougé, Z. Phys. C 70 (1996) 65.

[21] CLEO Collaboration, J. Bartelt et al., Phys. Rev. Lett. 76 (1996) 4119.

[22] CLEO Collaboration, M. Artuso et al., Phys. Rev. Lett. 69 (1992) 3278.

[23] ND Collaboration, V. P. Druzhinin et al., Phys. Lett. B 174 (1986) 115;
DM1 Collaboration, B. Delcourt et al., Phys. Lett. B 113 (1982) 93;
DM2 Collaboration, A. Antonelli et al., Phys. lett. B 212 (1988) 133.